Early Stage of Oxidation of Mo_3Si by In Situ Environmental Transmission Electron Microscopy

A. Gulec,* X.X. Yu,‡,* M. Taylor,** A. Yoon,*** J.M. Zuo,*** J.H. Perepezko,** and L.D. Marks‡,*

ABSTRACT

Mo-Si-based superalloys are of interest as a new family of high-temperature materials to replace Ni-based alloys. By means of in situ environmental transmission electron microscope, the transient period of the early oxidation of Mo_3Si was investigated at the nanometer scale. As a result of a competition between loss of volatile MoO_3 and association of SiO_2 molecular units into pillars, a nanometer-sized porous SiO_2 grows at a very initial stage of the oxidation of Mo_3Si.

KEY WORDS: in situ environmental transmission electron microscope (ETEM), Mo-Si-based superalloy, oxidation, porous

INTRODUCTION

Ni-based superalloys, which have been used in aerospace and power-generation gas-turbine engines operating at high temperatures, are serving near their melting point.[1-2] There is a drive to increase turbine inlet temperatures to increase overall efficiency, but the currently commercially used materials have reached their limits.[3-4] With a higher melting temperature, and favorable mechanical, creep, and oxidation properties, Mo-Si-B alloys based upon a multiphase microstructure of a Mo solid solution (Mo_{ss}), and the Mo_3Si and the Mo_5SiB_2 phases are good candidates for a new family of high-temperature alloys to replace the Ni-based alloys.[5-6] To date, the early stage of oxidation behavior of Mo-based alloys has been studied at the microscale,[7-8] but a complete analysis of the initial oxidation during what is termed in the literature as the transient period requires a description of the reaction at the nanometer scale level.

In the Mo-Si-B alloys, a higher Mo content provides fracture toughness and ductility, but the Mo-rich compositions have poor oxidation resistance. With an increased B content the oxidation resistance is improved at low temperature, but there is a loss of toughness and ductility. However, at elevated temperature B-rich Mo-Si-B alloys do not show good oxidation performance because of the loss of B through B_2O_3 evaporation. Si-rich Mo-Si-B alloys have excellent oxygen resistance performance at high temperature, but suffer from brittle behavior and at intermediate temperatures a pesting reaction.[5-6] To achieve a material with all of the desired properties for high-temperature applications, such as oxidation resistance, creep resistance, and strength at a wide range of temperatures, three-phase alloys comprising Mo, Mo_5SiB_2 (T_2 phase), and Mo_3Si (A15) have been explored by different processing methods to develop alternate multiphase microstructure morphologies.[5,7,9-10] There have been other attempts to improve the oxidation resistance of the Mo-Si-B system, including doping or alloying Mo-Si-B[11-13] and coating the Mo-Si-B alloy.[14-15]

On heating, there are four different oxidation regimes for Mo-Si-B alloys, each with a characteristic

Submitted for publication: June 21, 2017. Revised and accepted: October 18, 2017. Preprint available online: October 18, 2017, http://dx.doi.org/10.5006/2564.

‡ Corresponding author. E-mail: yuxx07@gmail.com (X.X. Yu), L-marks@northwestern.edu (L.D. Marks).
* Department of Materials Science and Engineering, Northwestern University, Evanston, IL 60208.
** Department of Materials Science and Engineering, University of Wisconsin-Madison, Madison, WI 53706.
*** Department of Materials Science and Engineering, University of Illinois, Urbana-Champaign, IL 61801.

ISSN 0010-9312 (print), 1938-159X (online)
18/000045/$5.00+$0.50/0

temperature range. Initial oxidation of Mo-Si-B alloys (Regime 1) starts at a relatively low temperature (~500°C) with parabolic weight gain resulting from solid oxide formation on the surface, which does not provide protection against continued oxidation. This is followed by Regime 2 with linear weight loss.[7,16] Between 650°C and 750°C (Regime 3), where the oxidation resistance is worst, the borosilica is not continuous over the surface and oxidation leads to a complete transformation into powder resulting from the loss of volatile MoO_3. This behavior is known as pesting. Above 750°C to 800°C (Regime 4), the borosilica reaction product can achieve a continuous scale, thus slowing down the oxidation and recession of the substrate.[7,16-18]

During the transient oxidation stage where the highest weight loss is observed, one key factor is the formation of viscous SiO_2 glass which forms a porous network of nano-channels that is a characteristic feature for oxidation of the Mo_3Si phase, as shown in Figure 1. These nano-channels consequently provide a pathway for oxygen diffusion to the substrate, enabling continued oxidation. The question which needs to be addressed for this stage of oxidation is what is the mechanism of porous silicon oxide formation. One possibility is the formation of a very thin layer of silicon oxide that is thin enough to allow oxygen diffusion through the substrate to create gaseous Mo oxide, which could then lead to nano-channels in the silicon oxide film. Another possible mechanism is the formation of initial nanoscale-sized islands, which coarsen to form a network of silicon oxide without a continuous coverage over the metal substrate.

If one could provide a homogenous boron distribution over the substrate, boron diffusion into the porous glass would lower the viscosity of the glass, which would lead to self-healing of the glass formed on the surface, which would then block further oxidation. Therefore, in addition to understanding of the initial interaction between the three phases, the initial stage of oxidation of the A15 phase is vital to elucidate in order to limit the transient stage of the oxidation and provide strong oxygen resistance. Mesoscopic descriptions of the early stage of oxidation, which do not capture what is actually happening in the near-surface selvedge region, have been reported,[7,18] but are at too large of a size scale. In this work, the very early stage of oxidation of the A15 phase was studied and the direct observation of nanometer size porous silicon oxide formation was reported by means of in situ environmental transmission electron microscope (ETEM) during the transient period. Faster silica formation at the grain boundaries was also observed as opposed to gradual silica formation away from the boundaries. The observations provide the basis for a model describing the initiation and evolution mechanism for the Mo_3Si phase oxidation.

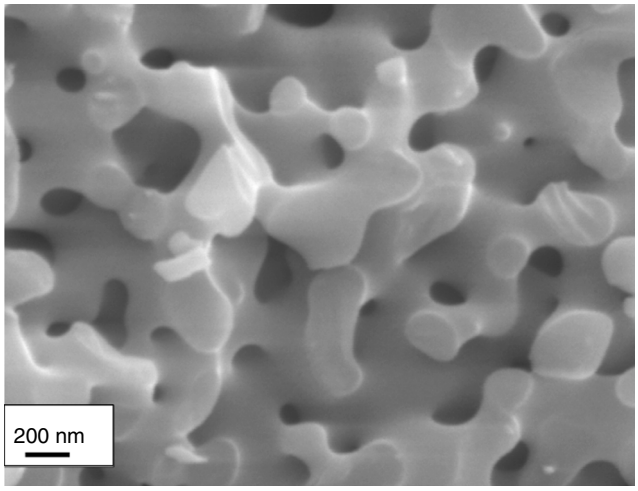

FIGURE 1. *Cross-sectioned Mo_3Si sample oxidized at 1,100°C in air for 10 min showing the porous silica formation. Reproduced from Rioult, et al.*[7]

EXPERIMENTAL DETAILS

Mo_3Si alloys were arc melted from 99.99% pure elemental reagents, with a total initial reagent mass of 10 g. To ensure homogeneity, the ingot was melted and re-melted five times, while measuring the ingot mass between each melt to monitor losses; only ingots with less than 1% total loss were used. For TEM analysis, the samples were polished using diamond lapping paper to remove the residual oxide on the surface. The powders were ground from the fresh surface without native oxide, and were attached to the tungsten wire of the specially designed TEM holder by a clean brush; the typical particle size was 100 nm. In situ oxidation experiments were performed using a Hitachi H-9500 ETEM[†] with a LaB_6 emitter operated at 300 kV. The special holder designed for the ETEM included a gas injection and heating environment directly on the sample.[19] Resistive heating was performed by passing an electric current though the tungsten wire. The temperature was determined using previous calibrations of the temperature versus electric current. After heating the sample above 800°C to equilibrate the surface, the temperature was decreased to the desired value and O_2 introduced into the TEM column at a pressure of 2×10^{-3} Pa. The images were recorded using an Orius SC200[†] camera from Gatan.

RESULTS

Figure 2 shows a bright-field ETEM image taken at 600°C. Before the oxygen is introduced, the surface shows no indication of residual oxide layer. After 15 min of oxygen exposure with a partial pressure of 2×10^{-3} Pa, dark features of about 1 nm in size appear superimposed on the bulk metal (in projection) and also at the edge of the sample superimposed on the

[†] Trade name.

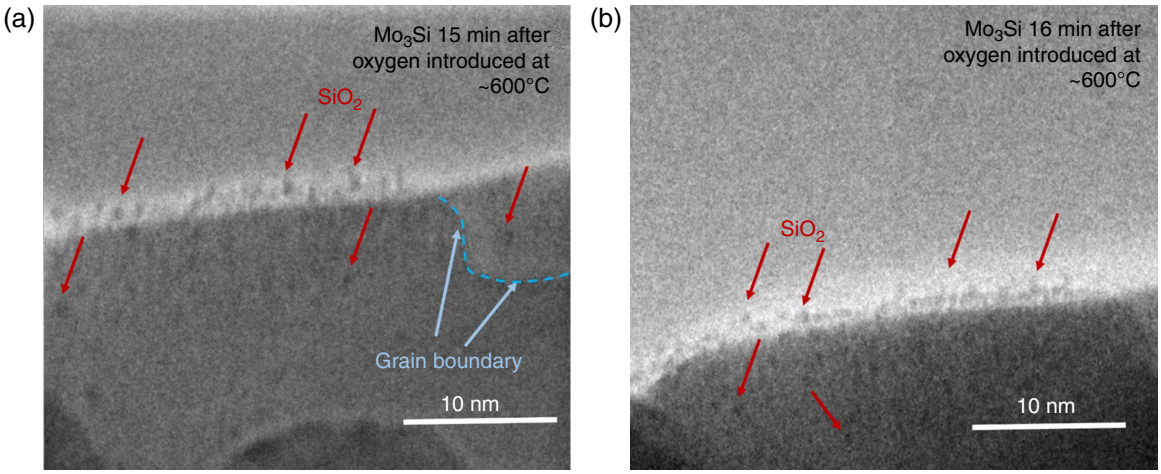

FIGURE 2. *In situ observation of oxide scale growth over the Mo_3Si substrate at 600°C. The porous nanosized SiO_2 scale is indicated with arrows. While they are more apparent at the profile edge (a), they can also be seen on the top/bottom of the bulk Mo_3Si phase (b).*

Fresnel fringe in the vacuum outside the Mo_3Si. A thin amorphous material does not show dynamical diffraction effects, e.g., Marks,[20] and is one of the exceptions where a simple mass-thickness analysis can be performed so long as Fresnel fringes resulting from defocus are taken into account. These darker regions can therefore be interpreted as small regions of amorphous silica, particularly as they all show approximately the same contrast, not the large variations from grain to grain that would be present for a nanocrystalline material. Isolated oxide islands develop initially as indicated by the arrows in the images, instead of a continuous thin oxide coverage over the surface. At this temperature, one would expect lower chemical activity and lower atomic diffusion in and out of the substrate. Therefore, the silica growth is slower, and the formation of MoO_x in the gas phase is also slower. While the oxide scales grow over time, they retain a nanoporous nature. Thus, at this temperature and oxygen partial pressure, the rate of MoO_3 evaporation is high compared to the rate of silica formation, so a fully dense, conformal (as against nanoporous) silica coverage of the substrate surface cannot be achieved.

The images are consistent with the high SiO_2 viscosity at 600°C preventing formation of a dense silica coverage over the surface. As discussed more later, there is a significant volume change, so considerable diffusion of the oxide would be needed to form a dense (as against porous) layer. One important observation is that there is no sign of faster oxide growth near the grain boundaries in Figure 2, which can be compared to the higher temperature results below. In addition, for the grain to the right in Figure 2(a), the oxide formation does not appear as thick as over the grain in the center of the image. Variation of the oxide growth for different grains implies a not unexpected dependence on the crystallographic orientation of the substrate surface.

The formation of SiO_2 may cause a local composition change in the selvedge region. In previous in situ studies of A15 oxidation, evidence for Mo-metal or MoO_2 formation in equilibrium with SiO_2 has been observed.[21] However, no indications of an underlying Mo zone are seen. This would show clearly as different contrast near the surface in the images. The experimental data are consistent with a high MoO_3 evaporation rate precluding the development of Mo enrichment, i.e., a Mo-metal scale does not form in this temperature and pressure regime during the early stage.

In Figure 3, the early oxidation stages of Mo_3Si are shown starting at 700°C. Before the oxygen is introduced into the microscope column, Mo_3Si grains with size of ~20 nm are observed and labeled as A, B, and C, respectively, in Figure 3(a) without any trace of oxide at 700°C. Three minutes after the oxygen was introduced into the column, as seen in Figure 3(b), the first oxide scales appear, with a thickness around 1 nm. These scales form on the grain boundaries between grains A and B and between grain B and grain C, which are labeled with arrows and dashed lines. As a function of time, there is minimal change in the grooving at the grain boundaries, rather, the formation of amorphous silica indicating that the grain boundaries act as preferential sites for the nucleation of the silica, as against being preferential sites for sublimation of Mo oxide which would be indicated by increased grooving at the boundaries. The rest of the surface, which is away from the grain boundaries, displays less oxide film growth. Solid MoO_x formation is not observed, which can be explained by the higher rate of evaporation of MoO_3 at this temperature compared to the oxide growth rate. Additionally, the surface region on grain B, where the MoO_3 evaporation occurs, is the region in between two grain boundaries

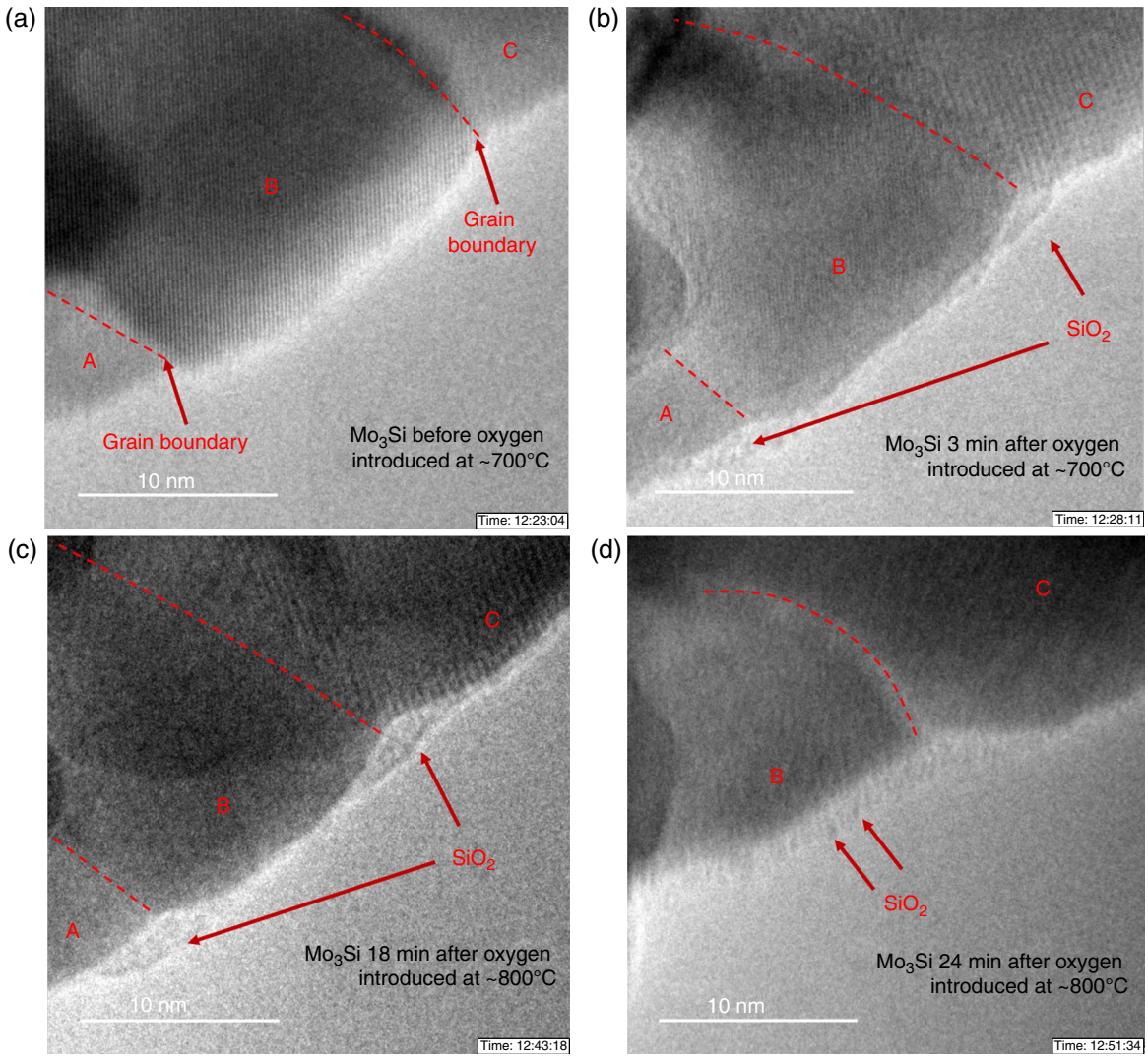

FIGURE 3. *In situ observation of oxide scale growth over the Mo_3Si substrate as function of time and temperature: (a) before oxidation, ([b] through [d]) during the oxidation. Three neighboring grains are labeled with nanoscale SiO_2 scales, indicated with arrows.*

where no SiO_2 growth is observed. After observing stable oxide thickness over the surface at 700°C, the temperature was increased to 800°C and the results are shown in Figures 3(c) and (d). In addition to the larger grain sizes, the oxide layer over the surface, near grain boundaries, initially becomes larger, which is expected considering the higher diffusion rate of Si and O at 800°C. Twenty-four minutes after the oxygen was introduced into the sample environment, the oxide layer near the grain boundaries spreads over the whole surface area, as seen in Figure 3(d). At this stage, the oxide layer contains nanometer-sized oxide pores. Similar to Figure 2, the image can be interpreted using a mass-thickness approach, and shows too much variation to be just a continuous amorphous film, and is different from how a nanocrystalline material would appear. The faster gaseous MoO_3 formation rate contributes to the open channels in the amorphous silica layer on top, forming a nanoporous scale. Another interesting observation is the difference in the oxide growth for grain B and grain C. The porous silica covers grain B completely, while the oxide growth on grain C is limited. This variation can be related again to the crystallographic orientation of the substrate surface. Additionally, taken before and after the oxidation, the electron diffraction results show no evidence of change in crystallographic structure of the Mo_3Si resulting from the oxidation.

Finally, a diffraction pattern after sample cooling in the TEM column is shown in Figure 4, which confirms the presence of amorphous SiO_2 mixed with MoO_3 and the Mo_3Si substrate. The existence of MoO_3 in the diffraction pattern is a result of further oxidation of Mo during cooling to room temperature.

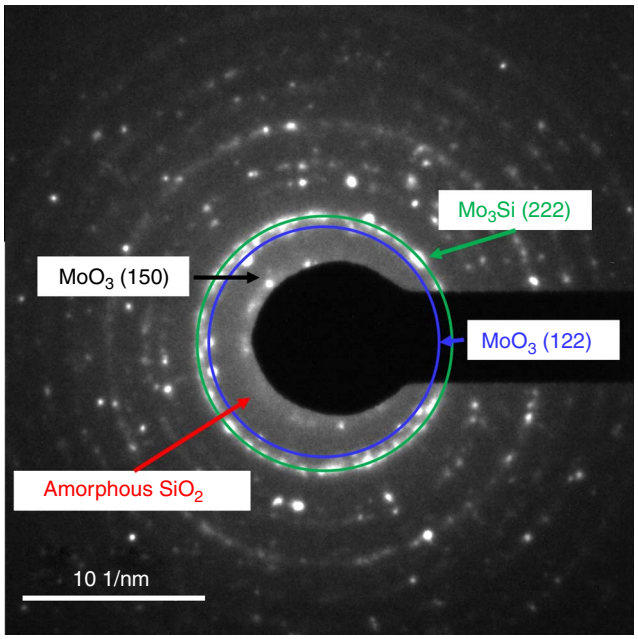

FIGURE 4. *Diffraction patterns taken after cooling the sample to room temperature, showing the presence of MoO_3 as a result of oxidation during cooling and (weak) diffuse rings consistent with amorphous silica.*

DISCUSSION

As mentioned in the introduction, the question which needs to be addressed to enable design of better oxidation resistance in the MoSiB family of high-temperature materials is what the mechanism is in the very early stages of oxidation which leads to more macroscopic porous silicon oxide formation. The experimental results indicate that for the temperatures studied, even at the earliest monolayer stages, the oxide film is nanoporous, although considering the scale "atomically-porous" would be a more descriptive term. This indicates that as the scale thickens, the larger pore sizes that have been described at the more macroscopic sizes are a consequence of Ostwald ripening of the pores simultaneous with thickening.

Some further analysis is useful. For single phase Mo_3Si there are only limited reports for the oxidation behavior. The effect of Al alloying on the oxidation of Mo_3Si in air at 1,000°C was examined by Rosales, et al.,[11] with only incomplete results for unalloyed samples. Similarly, Ochiai[22] focused on the effect of Cr and Al alloying on the oxidation of Mo_3Si at 900°C in air. From TGA measurements,[7] the linear oxidation rate for Mo_3Si was reported as 4.2 mg/cm^2·s at 1,100°C. Without specific data for the oxidation rate kinetics of Mo_3Si for the temperature range examined, it is instructive to consider the oxidation behavior in Mo for which data are available. For the oxidation of Mo over the temperature range from 550°C to

TABLE 1
Summary of the ETEM Observation

Temperature (°C)	
600	Oxide islands initiate; no continuous oxide film
700	Oxide film formation initiates near grain boundaries
800	Continuous porous silica forms over the surface

1,700°C, the mass loss rate per unit area (dM_{ox}/dt) is given by:[23]

$$\frac{dM_{ox}}{dt} = A \exp\left[\frac{-E}{RT}\right] \quad (1)$$

where A = 0.504 g/cm^2·s, E = 82.4 kJ/mol, R is the gas constant, and T is the temperature. The values of (dM_{ox}/dt) are listed in Table 1 for 600°C, 700°C, and 800°C. To evaluate the suitability of using Equation (1), the calculated oxidation rate at 1,100°C of 0.5 mg/cm^2·s can be compared to the reported rate of 0.07 mg/cm^2·s. Thus, Equation (1) gives a conservative overestimate of the oxidation rate. For the oxidation product of MoO_3, the vapor pressure, P, for solid MoO_3 is represented by:[24]

$$\ln P = \frac{-315{,}473}{RT} + 31.36 \quad (2)$$

where P is the absolute pressures, $\Delta H_{s\text{-}v}$ = 315,473 J/mol is the enthalpy of sublimation, R is the gas constant, and T is the temperature. Above the melting point of MoO_3 at 795°C, the vapor pressure is given by:[24]

$$\ln P = \frac{-147{,}276}{RT} + 12.38 \quad (3)$$

where the enthalpy of vaporization $\Delta H_{l\text{-}g}$ = 147,276 J/mol. The vapor pressures are listed in Table 2. The rate of mass loss per unit area (dM_{evap}/dt) by MoO_3 evaporation can be evaluated by the Langmuir equation,

$$\frac{dM_{evap}}{dt} = P\left[\frac{m}{2\pi RT}\right]^{0.5} \quad (4)$$

where m is the molecular weight. For MoO_3, the dominant vapor species is reported as $(MoO_3)_{\#}$.[24] The

TABLE 2
Calculated Mass Loss Rate Per Unit Area as a Result of Oxidation and Evaporation at Several Temperatures

Temperature (°C)	(dM_{ox}/dt) (g/cm^2·s)	P (Pa)	(dM_{evap}/dt) (g/cm^2·s)
600	5.93×10^{-6}	0.548	2.53×10^{-7}
700	1.89×10^{-5}	47.9	2.18×10^{-5}
800	4.92×10^{-5}	1,618	6.73×10^{-4}

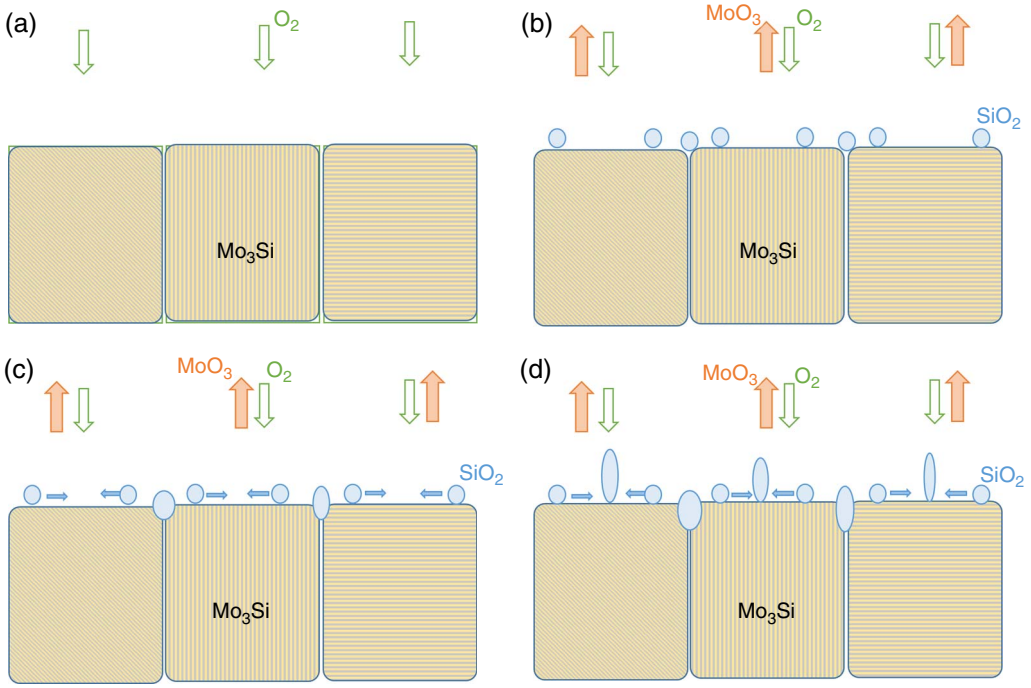

FIGURE 5. *Illustration of this mechanism for the development of the nanoporous SiO_2 morphology. (a) Initial exposure to O_2, (b) chemisorption leads to formation of SiO_2 molecular units along with evaporation of MoO_3, (c) linkage of SiO_2 units to form a nanoporous network along with silica development at grain boundaries and continued evaporation of MoO_3, and (d) coalescence of SiO_2 units into pillars with continued evaporation of MoO_3 and thickening of grain boundary silica.*

resultant values for (dM_{evap}/dt) are also listed in Table 2. It is evident from the mass loss rates listed in Table 2 that the loss resulting from evaporation is greater than that resulting from oxidation above 700°C. Thus, oxidation is the rate limiting step in the formation and removal of MoO_3 during reaction.

With the oxidation of Mo and removal of MoO_3 from the Mo_3Si surface, the exposed Si will oxidize to SiO_2. If the mobility of the SiO_2 is high one would expect a conventional growth (Volmer-Weber, Stranski-Krastanov, or layer-by-layer[25]) of the oxide film, but this was not observed. Over the temperature range of 600°C to 800°C, the viscosity of bulk SiO_2 is much too high to account for the evolution of the nanoporous SiO_2 morphology by flow.[26] Indeed, if there were complete coverage, the escaping MoO_3 gas would cause bubble formation and disrupt the SiO_2 film which was not observed for in situ experiments with thicker oxide films,[18] but has been observed in three phase (Mo + Mo_3Si + Mo_5SiB_2) alloys with different compositions.[16-17,27]

Instead, the nanoporous (atomically-porous) film develops even at a thickness of 1 nm to 2 nm. In the A15 Mo_3Si starting material, the volume per Si atom is 5.87×10^{-2} nm^3, taking quartz as a reference for the oxide it would be 3.77×10^{-2} nm^3, about two-thirds the volume. Further, for the oxidation reaction for Mo_3Si given by:

$$Mo_3Si + 11/2O_2 \rightarrow SiO_2 + MoO_3 \quad (5)$$

The molar volumes for Mo_3Si, SiO_2, and MoO_3 are 27.3 cm^3/mol, 35.1 cm^3/mol, and 30.7 cm^3/mol, respectively. Because MoO_3 is lost by vaporization, the 22% decrease in volume upon oxidation indicates that complete coverage by the silica product is not possible. This model is illustrated in Figure 5. Figure 5(b) shows that relatively isolated SiO_x molecular units (monomers) effectively chemisorbed onto the base A15 Mo_3Si do not migrate extensively; rather, they crosslink to form the porous network right from the first monolayers. As the oxidation proceeds there will be slow Ostwald ripening of the porous network, assisted by surface diffusion across the existing SiO_2 surfaces of the SiO_x monomers freshly created by MoO_3 sublimation from exposed Mo_3Si surfaces. This will tend to create pillars, but Rayleigh instabilities will lead to a three-dimensional porous network by creating cross-connects as reported in the literature for thicker regions of the silicate.

CONCLUSIONS

❖ The present work shows direct observation of the initial stage of oxidation of Mo_3Si at various elevated temperature by in situ environmental TEM. Nanoscale porous SiO_2 formation at 600°C and 800°C without formation of a continuous oxygen resistant silica surface was observed. The silica formation starts with nanoscale oxides and leads to a network over the

substrate rather than forming a thin silica film which later converts to a porous structure as a result of MoO_3 gas bubble formation. These findings also indicate that faster atomic migration through the grain boundaries allows formation of thicker non-porous SiO_2 on the surface of the substrate near the grain boundaries around 700°C, which potentially slows down the weight loss during the transient oxidation stage. The proposed oxidation step model indicates that to increase the oxidation resistance, the Mo_3Si phase should be modified to promote additional oxides and to enhance the fluidity of the silica to yield complete surface coverage from the earliest stage of oxidation.

ACKNOWLEDGMENTS

The authors acknowledge support from ONR MURI "Understanding Atomic Scale Structure in Four Dimensions to Design and Control Corrosion Resistant Alloys" on Grant No. N00014-14-1-0675. The in situ TEM performed at UIUC was partially supported by NSF DMR-1410596 (A.Y. and J.M.Z.) and the Hitachi H9500 ETEM was supported by NSF MRI-1229454.

REFERENCES

1. T.M. Pollock, S. Tin, *J. Propul. Power* 22, 2 (2006): p. 361-374.
2. R.C. Reed, *The Superalloys: Fundamentals and Applications* (Cambridge, United Kingdom: Cambridge University Press, 2008).
3. B.P. Bewlay, M.R. Jackson, P.R. Subramanian, J.-C. Zhao, *Metall. Mater. Trans. A* 34, 10 (2003): p. 2043-2052.
4. N. Saunders, "Rolls Royce PLC Report PNR," 1996.
5. D.M. Dimiduk, J.H. Perepezko, *MRS Bull.* 28, 9 (2003): p. 639-645.
6. J.A. Lemberg, R.O. Ritchie, *Adv. Mater.* 24, 26 (2012): p. 3445-3480.
7. F.A. Rioult, S.D. Imhoff, R. Sakidja, J.H. Perepezko, *Acta Mater.* 57, 15 (2009): p. 4600-4613.
8. B. Roy, J. Das, R. Mitra, *Corros. Sci.* 68 (2013): p. 231-237.
9. D.M. Berczik, "Method for Enhancing the Oxidation Resistance of a Molybdenum Alloy, and a Method of Making a Molybdenum Alloy," U.S. Patent US5595616 A, 1997.
10. R. Sakidja, J.H. Perepezko, S. Kim, N. Sekido, *Acta Mater.* 56, 18 (2008): p. 5223-5244.
11. I. Rosales, H. Martinez, D. Bahena, J.A. Ruiz, R. Guardian, J. Colin, *Corros. Sci.* 51, 3 (2009): p. 534-538.
12. T. Sossaman, J.H. Perepezko, *Corros. Sci.* 98 (2015): p. 406-416.
13. S. Majumdar, B. Dönges, B. Gorr, H.-J. Christ, D. Schliephake, M. Heilmaier, *Corros. Sci.* 90 (2015): p. 76-88.
14. A. Lange, R. Braun, *Corros. Sci.* 84 (2014): p. 74-84.
15. A. Lange, M. Heilmaier, T.A. Sossamann, J.H. Perepezko, *Surf. Coat. Technol.* 266 (2015): p. 57-63.
16. T.A. Parthasarathy, M.G. Mendiratta, D.M. Dimiduk, *Acta Mater.* 50, 7 (2002): p. 1857-1868.
17. M. Mendiratta, T. Parthasarathy, D. Dimiduk, *Intermetallics* 10, 3 (2002): p. 225-232.
18. D.A. Helmick, G.H. Meier, F.S. Pettit, *Metall. Mater. Trans. A* 36, 12 (2005): p. 3371-3383.
19. X.F. Zhang, T. Kamino, *Microsc. Today* 14 (2006): p. 16.
20. L.D. Marks, *Ultramicroscopy* 25, 1 (1988): p. 85-87.
21. R. Sakidja, J.S. Park, J. Hamann, J.H. Perepezko, *Scrip. Mater.* 53, 6 (2005): p. 723-728.
22. S. Ochiai, *Intermetallics* 14, 10-11 (2006): p. 1351-1357.
23. E.A. Gulbransen, K.F. Andrew, F.A. Brassart, *J. Electrochem. Soc.* 110, 9 (1963): p. 952-959.
24. E.A. Gulbransen, K.F. Andrew, F.A. Brassart, *J. Electrochem. Soc.* 110, 3 (1963): p. 242-243.
25. A. Pimpinelli, J. Villain, *Physics of Crystal Growth* (New York, NY: Cambridge University Press, 1998).
26. R.H. Doremus, *J. Appl. Phys.* 92, 12 (2002): p. 7619-7629.
27. P. Marshall, "Development of Oxidation Resistant Molybdenum-Silicon-Boron Composites" (Ph.D. diss., Georgia Institute of Technology, 2015).